SpirDet: Towards Efficient, Accurate and Lightweight Infrared Small Target Detector

Qianchen Mao, Qiang Li, Bingshu Wang*, Yongjun Zhang, Tao Dai, C.L. Philip Chen, Fellow, IEEE

Abstract—In recent years, the detection of infrared small targets using deep learning methods has garnered substantial attention due to notable advancements. To improve the detection capability of small targets, these methods commonly maintain a pathway that preserves high-resolution features of sparse and tiny targets. However, it can result in redundant and expensive computations. To tackle this challenge, we propose SpirDet, a novel approach for efficient detection of infrared small targets. Specifically, to cope with the computational redundancy issue, we employ a new dual-branch sparse decoder to restore the feature map. Firstly, the fast branch directly predicts a sparse map indicating potential small target locations (occupying only 0.5% area of the map). Secondly, the slow branch conducts finegrained adjustments at the positions indicated by the sparse map. Additionally, we design an lightweight DO-RepEncoder based on reparameterization with the Downsampling Orthogonality, which can effectively reduce memory consumption and inference latency. Extensive experiments show that the proposed SpirDet significantly outperforms state-of-the-art models while achieving faster inference speed and fewer parameters. For example, on the IRSTD-1K dataset, SpirDet improves MIoU by 4.7 and has a $7 \times FPS$ acceleration compared to the previous state-of-the-art model. The code will be open to the public.

Index Terms—Article submission, IEEE, IEEEtran, journal, LaTeX, paper, template, typesetting.

I. Introduction

Infrared small target detection holds significant potentials for various applications [1], [2], [4], such as maritime rescue [6], [7] and urban security [8]. In these situations, it is vital for

This work is supported by the National Natural Science Foundation of China, Youth Fund, under number 62102318, and the Basic Research Programs of Taicang, 2023, under number TC2023JC23. This work is also funded in part by the National Natural Science Foundation of China grant under number 92267203, in part by the Science and Technology Major Project of Guangzhou under number 202007030006, and in part by the Program for Guangdong Introducing Innovative and Entrepreneurial Teams (2019ZT08X214). (Corresponding author: Bingshu Wang.)

Qianchen Mao is with the School of Software, Taicang Campus, Northwestern Polytechnical University, Suzhou 215400, China (e-mail:mqc@mail.nwpu.edu.cn).

Qiang Li is with the School of Software, Taicang Campus, Northwestern Polytechnical University, Suzhou 215400, China (e-mail: lq2023@mail.nwpu.edu.cn).

Bingshu Wang is with the School of Software, Northwestern Polytechnical University, Xi'an 710129, China, and National Engineering Laboratory for Big Data System Computing Technology, Shenzhen University, Shenzhen 518060, China. (e-mail: wangbingshu@nwpu.edu.cn).

Yongjun Zhang is with the State Key Laboratory of Public Big Data, College of Computer Science and Technology, Guizhou University, Guiyang 550025, Guiyang, China. (e-mail: zyj6667@126.com).

Tao Dai is with the College of Computer Science and Software Engineering, Shenzhen University, Shenzhen 518060, China (e-mail:daitao.edu@gmail.com).

C. L. P. Chen is with the School of Computer Science and Engineering, South China University of Technology and Pazhou Lab, Guangzhou 510641, 510335, China (e-mail: philip.chen@ieee.org).

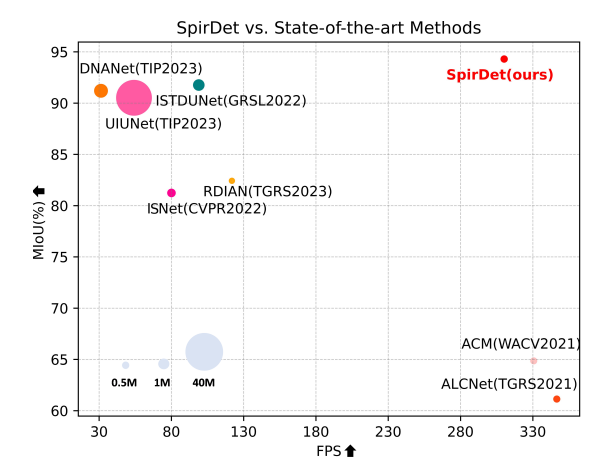


Fig. 1: The MIoU, FPS versus model size on NUDT-SIRST [33] test set. Our SpirDet are marked as red point. As can be seen from the comparison, our SpirDet achieves a better FPS/MIoU. All the frame per second(FPS) were measured on a single NVIDIA RTX 3090, with an input size of 256×256 .

the detectors to identify targets while ensuring both high accuracy and enhanced inference speed [9]. Hence, investigating a high-performance and efficient infrared small target detector is a prominent area of focus.

Infrared sensors capture solely thermal radiation signals, leading to images lacking of details [5]. It is necessary for an infrared small target detector to discern targets from a significant distance. As a result, these targets typically occupy the image only a sparse number of pixels, ranging from a few to several tens. This forms two characteristics of infrared small targets: 1) small and weak [10], [11], due to their minute size, discernible texture, shape, and other target information are significantly diminished. 2) low signal-to-noise ratio [12]–[14], the abundance of noise interference within infrared images can lead to false identification of background interference as targets.

Early detection of infrared small targets are model-based methods [36]–[38], leveraging human prior knowledge for detection and offering commendable real-time performance. Nonetheless, these methods are significantly impeded by the hand-crafted features, resulting in poor generalization, low accuracy and high false detection rates. Recent advancements redefine infrared small target detection as a semantic segmentation task [28], [39], [40], utilizing architectures such as Unet series [15]. Given that the targets occupy only a sparse subset of the image's pixels, there is a potential risk of spatial

information loss during the down-sampling phase within the encoder. To enhance the performance of small target detection, some methods [33]–[35] maintain a high-resolution feature map pathway between the encoder and decoder. However, as the feature map size increases, the computational cost grows quadratically.

The motivation of this paper is to focus computations on the potential positions of small targets within high-resolution (HR) feature maps for tasks necessitating high resolution, such as edge detection and shape learning of small targets. To achieve high speed and superior performance, this paper introduces SpirDet, which capitalizes on several distinctive characteristics of infrared small targets. We propose the Dual-branch Sparse Decoder(DBSD). This decoder utilizes a fast branch to predict the coarse-grained positions of small targets on low-resolution feature maps directly, followed by a slow branch that employs sparse convolution to refine the positions within these coarsegrained regions on an HR level. This refinement compensates for performance degradation experienced when restoring lowresolution maps to their original scale. Furthermore, we design a reparameterized Encoder, termed DO-RepEncoder, which boasts a large model capacity while preserving a high inference speed.

As shown in Fig. 1, our SpirDet appreciably improves Mean Intersection over Union (MIoU) while markedly reducing inference latency. It surpasses existing methods for infrared small target detection in terms of metrics such as the false alarm rate (F_a) , probability of detection (P_d) , and Frames per Second(FPS).

Our contributions can be summarized as follows:

- We propose a high-performance and high-speed network architecture called SpirDet for infrared small target detection. It incorporates a reparameterization module into DO-RepEncoder to maintain model capacity while substantially accelerating model inference speed.
- We present a Dual-branch Sparse Decoder (DBSD) including fast and slow branch. The fast branch produces a sparse map of potential target positions and guides the slow branch for high-resolution and fine-grained refinement. This can reduce computation costs of model largely.
- ullet Experiments conducted on the NUDT-SIRST [33] dataset demonstrate that the SpirDet exceeds the state-of-the-art (SOTA) by 2.09%, accompanied by a threefold increase in FPS. Similarly, on the IRSTD-1K [31] dataset, SpirDet attains SOTA results with a 4.74% improvement, boasting an FPS that is $7\times$ higher than the previous SOTA.

II. RELATED WORK

A. Infrared Small Target Detection

The prevailing trends in Infrared Small Target Detection (IRSTD) coalesce into two principal categories: model-based methods and data-driven methods. Model-based methods [51], [53] leverage artificial prior knowledge for detection, encompassing strategies that suppress backgrounds [16], [17], construct models informed by the human visual system [19]–[21], [36], [50], [52], and employ optimization-based techniques [23], [24]. Despite their ability to execute swiftly on

edge devices, these methods frequently fall short in terms of generalization capability in complicated scenarios.

Conversely, the latter category interprets IRSTD as a semantic segmentation problem underpinned by deep learning [43], [44], [46], [48], [56]. Some approaches [29], [30], [34], [35], [54] capture high-level semantic features via cross-level feature fusion to obtain high-resolution, detailed small target features. Another strain of methods concentrates on improving the learning of small target context information representation [42], generally employing Attention mechanisms [32], [33], [45], [47], [49], [55]. In addition, certain methods direct the network's focus on the edges and shape information of infrared small targets, thereby enabling more accurate representation of the small target.

Data-driven methods have demonstrated superior results compared to model-based methods. However, these methods grapple with achieving a balance between speed and performance due to the conflict between high-resolution small target feature learning and low network inference latency. In this paper, we address this contradiction through the implementation of sparse convolution.

B. Sparse Convolution Network

Sparse convolution networks have recently been recognized as an effective technique for managing tasks predicated on sparse prior knowledge. For example, Yan *et al.* [58] utilized 3D sparse convolution in the 3D object detection with voxel representation, jump over non-object features and thereby increasing the speed of network inference. In the realm of target detection, Yang *et al.* [57] employed sparse convolution to pinpoint small targets within the high-resolution feature maps of the FPN [61]. Du *et al.* [59] trained masks using the Gumbel-Softmax [60] trick, leading to the adaptive acceleration of heavy detection heads via sparse convolution.

In this paper, sparse convolution network is incorporated into IRSTD. By learning the sparse map of potential small target locations in the low-resolution feature map of the Decoder, we guide sparse convolution to specifically fine-tune the high-resolution information of small targets.

III. METHOD

A. Overall Architecture

The overall architecture of the proposed SpirDet is illustrated in Fig. 2. It comprises DBSD and DO-RepEncoder. The network takes an infrared image $\mathbf{X} \in \mathbb{R}^{1 \times H \times W}$ as input and initially reformats it to the required input shape using the Input Stem, as depicted in Fig. 2 (a). The DO-RepEncoder, composed of four stages of RepBlocks, performs downsampling using 3×3 convolutions in the first block of RepBlock. Following this, the feature maps P_i at varying levels undergo an upsampling process and lightweight fusion operations to capture multi-scale and contextual information. As demonstrated in Fig. 2 (b), the lightweight fusion concatenates P_{l+1} with the shallower feature maps, succeeded by a 3×3 convolution, batch normalization (BN), and ReLU activation, before direct addition to P_l . Finally, the DBSD processes the feature maps, incorporating a Fast-Slow Dualbranch, to output the final result O.

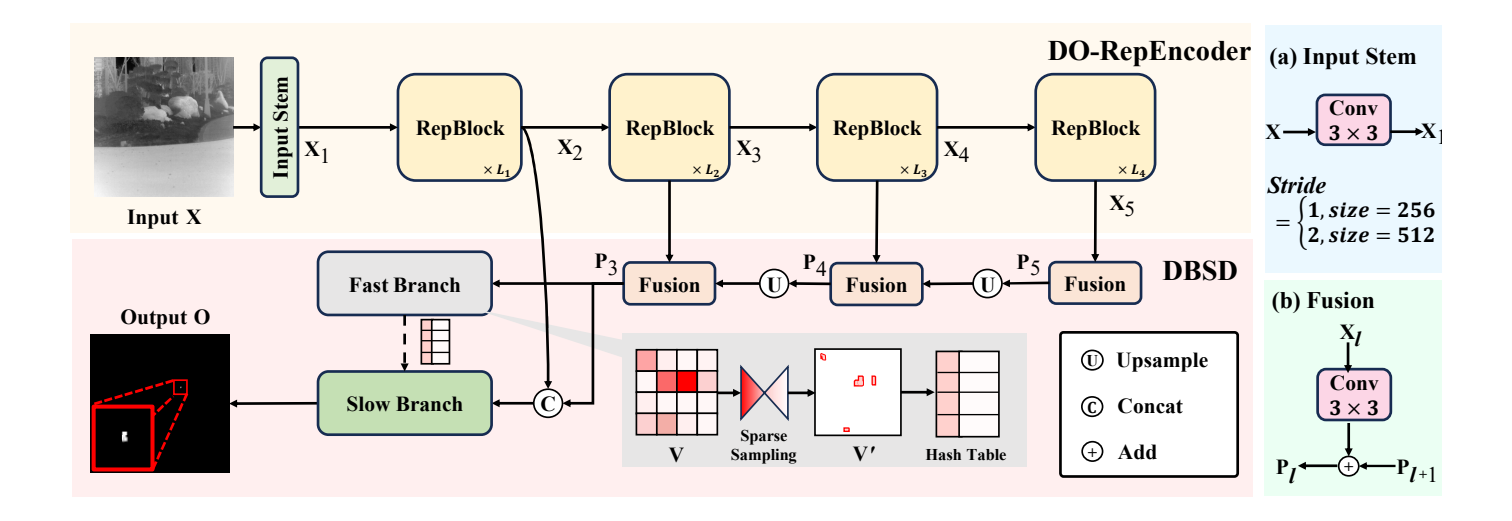


Fig. 2: The overall architecture of the proposed SpirDet, which comprises DO-RepEncoder and Dual-branch Sparse Decoder.

B. Dual-branch Sparse Decoder

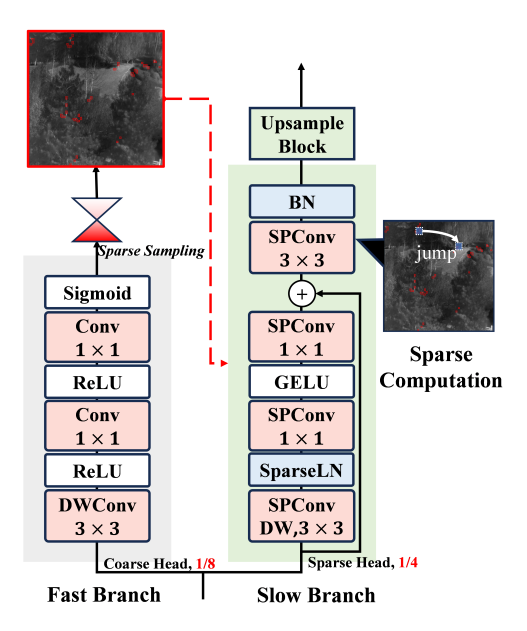


Fig. 3: The structure diagram of the DBSD. The term 'Sparse Computation' signifies that the sparse convolution operates exclusively at significant locations. 1/8 and 1/4 denote one-eighth and one-fourth of the original resolution, respectively. The red areas in the image represent potential small target locations.

To mitigate the potential loss of small target features when downsampling, prevalent architectures of infrared small target detectors typically sustain a high-resolution feature map pathway to secure clear target features. However, the distribution of infrared small targets within images is generally extremely sparse. An intuitive approach is to restrict computations exclusively to target-related features, automatically bypassing target-irrelevant features when convolution operates on the feature maps. The computation guided by this approach partially

resolves the significant imbalance issue between foreground and background classes that is frequently encountered in infrared small target detection.

In this section, we introduce the Dual-branch Sparse Decoder (DBSD), which incorporates both the *fast branch* and the *slow branch*. The *fast branch*, outfitted with the *coarse head*, swiftly predicts the coarse-grained potential locations of small targets with minimal computational costs on lower-resolution feature maps. These potential locations are then subjected to *sparse sampling* to yield a sparse binary mask with a low ratio (for instance, 0.5% of the entire image). The sparse binary mask is further transformed into a Hash Table indicating the positions. This hash table directs the *sparse head* of the *slow branch* to execute concentrated computations on the potential locations of small targets on higher-resolution feature maps. Subsequently, the predicted feature map is returned to the original resolution via the *upsample block*. The implementation specifics of DBSD are depicted in Fig. 3.

The fast branch is engineered to acquire the sparse mask. For instance, when given an original resolution input $\mathbf{X} \in \mathbb{R}^{1 \times H_l \times W_l}$, the coarse head accepts a lower-resolution feature map $\mathbf{P_1} \in \mathbb{R}^{C_l \times H_l \times W_l}$ from the l-th layer of the decoder, producing a probability map $\mathbf{V} \in \mathbb{R}^{1 \times H_l \times W_l}$ that signifies the likelihood of the grid $\mathbf{V}_{i,j}$ being associated with an infrared small object. Here, C_l , H_l , and W_l denote the number of channels, height, and width of the l-th layer, respectively. To streamline the prediction task of the coarse head, we employ the SoftIoU loss to supervise the output probability map \mathbf{V} as:

$$\mathcal{L}_{sparse}(\mathbf{V}, \mathbf{GT}) = 1 - SoftIoU(\mathbf{V}, Maxpool(\mathbf{GT})), \quad (1)$$

where the coarse-grained ground truth (GT) is derived using the Maxpooling operator. Consequently, the coarse head can confidently predict the probability map \mathbf{V} of potential small object locations. The probability map \mathbf{V} then undergoes TOP-K filtering, retaining only the grids exhibiting the highest confidence to form a sparse binary map

Fig. 4: The framework of RepBlock. It is composed of *N* blocks, each of which contributes to a multi-branch structure during the training phase and is reparameterized into a single-branch structure in the inference phase.

 $\mathbf{V}^{'} \in \{0, 1\}^{1 \times H \times W}$, where a hyperparameter α (e.g., 0.5%) determines the retention ratio of \mathbf{V} . This step is referred to as *sparse sampling*:

$$\mathbf{V}_{i,j}^{'} = \begin{cases} 1 & \text{if i, j} \in \text{TOP-K}(\mathbf{V}, \alpha \times H \times W) \\ 0 & \text{otherwise} \end{cases}, \quad (2)$$

where the TOP-K returns the 2D coordinates of the filtered grid.

The motivation for *sparse sampling* is twofold: (1) managing the scale of the overall sparse region, which only has a noticeable acceleration effect when scale is small, and (2) utilizing α to control the range of the context region related to small targets. Because infrared small targets are exceedingly small, the context region genuinely associated with the target is also extremely sparse. Thus, by adjusting α , the context region related to small targets can be compressed drastically. The performance metrics are substantially influenced by the hyperparameter α , which will be discussed in the experimental section.

The *slow branch* ingests a higher-resolution feature map, denoted as P_{l-1} , and generates a probability map that matches the original resolution. Subsequently, P_{l-1} is dispatched to the sparse head, an efficient component that capitalizes on sparse convolution. This type of convolution selectively operates on the foreground region using the sparse binary mask V, as detailed in Eq. 2. Throughout the network inference process, convolution is strictly applied where the mask value is 1. This strategic utilization of sparsity significantly reduces computational requirements when processing high-resolution target-related features. Unlike traditional convolutions, which uniformly compute on each grid of the feature map, the sparse head's computation exhibits spatial variation. It directly processes information related to small targets, taking advantage of the region of interest (ROI) role played by the sparse map V'. This approach enables it to more effectively learn intricate details such as shape. The sparse head further reduces computation by utilizing efficient combinations of DWConv and PWConv, and subsequently integrates spatial and channel information using a 3×3 Conv. Ultimately, the feature map generated by the sparse head is combined with a straightforward 1-Conv+1-Bilinear operation to produce the output $\mathbf{O} \in \mathbb{R}^{B \times 1 \times H_l \times W_l}$.

C. DO-RepEncoder

To reach a trade-off between model performance and inference speed, we introduce the reparameterization technique to satisfy model capacity and speed. Inspired by [62], [63], we design the DO-RepEncoder for feature extraction as shown in Fig. 4. The DO-RepEncoder consists of stages at different resolutions, with each Stage i containing L_i RepBlocks. Each RepBlock incorporates a Depthwise part and a Pointwise part, the former featuring a 3×3 convolution and the latter, a 1×1 convolution, both comprising a K parallel convolutions branch, which is represented by:

$$RepBlock(\mathbf{X}_i) = Pointwise(Depthwise(\mathbf{X}_i)). \tag{3}$$

During training, the Depthwise part caculated as below:

Depthwise(
$$\mathbf{X}_i$$
) = $ReLU(BN(\mathbf{X}_i)$
+ $\sum_{k}^{K} BN(3 \times 3DWConv_k(\mathbf{X}_i))$ (4)
+ $BN(1 \times 1DWConv(\mathbf{X}_i))$).

During inference, it transitions to a single-branch structure, ensuring the model's speed:

Depthwise(
$$\mathbf{X}_i$$
) = $ReLU(3 \times 3DWConv(\mathbf{X}_i))$. (5)

The multi-branch design during training enhances the overall model capacity.

To prevent the diminution of small object features during the downsampling process, we propose a *downsampling orthogonality* method by incorporating *orthogonality regularization* [64], [65] into the initial downsampling block of each stage, advocating for orthogonal weights among the K parallel convolutions:

$$\mathcal{L}_{orth}(\mathbf{W_{down}}) = \left\| \mathbf{W_{down}}^T \mathbf{W_{down}} - I \right\|_F^2, \quad (6)$$

where $\mathbf{W_{down}} \in \mathbb{R}^{(out \times K) \times in \times 3 \times 3}$ is

$$\mathbf{W_{down}} = Concat(W_1, W_2, ..., W_K). \tag{7}$$

Incorporating downsampling orthogonality(DO) as a regularization term in the final loss function ensures that the K parallel convolutions in downsampling, along with their distinct channels, are responsible for extracting different features

during network training. During inference, these K parallel convolutions, which extract diverse features, can be reparameterized into a single convolution. As a result, *downsampling orthogonality* achieves the aim of encoding diverse features of small objects using only one downsampling convolution during model inference.

D. Loss Function

The multi-task loss function of the proposed SpirDet predominantly comprises three components: (1) Output SoftIoU Loss \mathcal{L}_{Output} , which measures the discrepancy between the final output O of SpirDet and the Ground Truth. (2) Sparse SoftIoU Loss \mathcal{L}_{Sparse} , which quantifies the difference between the coarse-grained probability map V, generated by the *coarse* head of the DBSD, and the coarse-grained Ground Truth. (3) The orthogonality regularization loss \mathcal{L}_{orth} , which acts as a regularization term within downsampling orthogonality. Consequently, the aggregate loss function can be expressed as:

$$\mathcal{L}_{all} = \mathcal{L}_{Output} + \mathcal{L}_{Sparse} + \mathcal{L}_{orth}. \tag{8}$$

IV. EXPERIMENT

Table I presents the four publicly accessible infrared small target datasets utilized in our experiments: NUDT-SIRST [33], IRSTD-1K [31], SIRST3, and NUST [28]. SIRST3 is an amalgamated dataset from the NUAA-SIRST [29], NUDT-SIRST [33], and IRSTD-1K [31] datasets. For the NUST [28] dataset, we randomly divide it into train set(80%) and test set(20%).

Dataset	Resolution	Maximum	Average	Train/Test
NUDT-SIRST	256	0.27%	0.066%	664/665
IRSTD-1K	512	0.68%	0.028%	801/202
SIRST3	multiscale	0.68%	0.052%	1677/1080
NUST	128	1.07%	0.239%	7895/1998

TABLE I: Attributes of publicly accessible infrared small target datasets: Resolution: image size; Maximum, Average: the maximum and average proportions of small targets within the dataset. Train/test: the number of images.

A. Implementation Details

All models' training and experimental procedures were executed on an NVIDIA GeForce RTX 3090 GPU. For the IRSTD-1K [31], NUDT-SIRST [33], SIRST3, and NUST [28] datasets. We adhered to a training schedule of 400, 3000, 3000, and 2000 epochs for those datasets, respectively. The AdamW optimizer was utilized, accompanied by Cosine Annealing for learning rate decay, with an initial value of 0.0015 decaying to a minimum of 0.0005. For the multi-scale SIRST3 dataset, all images were uniformly resized to a 256×256 resolution for the experiments. We assessed model performance employing the pixel-level metric of Mean Intersection over Union (MIoU), object-level metrics of probability of detection (P_d) and Falsealarm rate (F_a), and evaluated model speed in terms of FPS.

Table II illustrates that our proposed SpirDet incorporates detail configurations to cater to infrared small target detection

SpirDo	lr	t	S	m	
	512×512	-	1	1	2
	256×256	4	2	4	6
Num. of Blocks	128×128	2	2	4	8
	64×64	2	1	1	1
	32×32	1	-	-	-
Num. of Spar	Num. of SparseConvs			4	4

TABLE II: Detail configurations of SpirDet. 'Num. of Blocks' denotes the number of blocks within each RepBlock, while 'Num. of SparseConvs' signifies the count of sparse convolutions in the SparseHead.

across varying resolutions. The 'lr' configuration is tailored for low resolution, corresponding to the NUDT-SIRST [33], SIRST3, and NUST [28] datasets. The 't', 's', 'm' configurations are designed to manage high-resolution data exceeding 512×512 , such as the IRSTD-1K [31] dataset, and respectively symbolize the tiny, small, and medium variants of SpirDet.

	Methods	Venue	Params		IRSTD	-1K	
	Methods	venue	Params	$MIou \uparrow$	$FPS \uparrow$	$P_d \uparrow$	$F_a \downarrow$
	Top-Hat	OE1996	-	10.06	-	75.11	143.20
	Max-Median	SPIE1999	-	7.003	-	65.21	5.97
	RLCM	GRSL2018	-	14.62	-	65.66	1.79
	WSLCM	GRSL2021	-	0.98	-	70.02	1502.70
	TLLCM	GRSL2019	-	5.36	-	63.97	0.49
1	MSLCM	IPT2018	-	5.34	-	59.93	0.54
1	MSPCM	IPT2018	-	7.33	-	60.27	1.52
	IPI	TIP2013	-	27.92	-	81.37	1.61
	NRAM	RS2018	-	15.24	-	70.67	1.69
	RIPT	JSTARS2018	-	14.10	-	77.54	2.83
	PSTNN	RS2019	-	24.57	-	71.98	3.52
	MSLSTIPT	RS2023	-	11.43	-	79.02	152.40
	ACM	WACV2021	0.40	59.15	162.59	90.57	2.04
	ALCNet	TGRS2021	0.43	61.59	214.99	89.56	1.44
	ISNet	CVPR2022	0.97	61.85	28.41	90.23	3.15
	RDIAN	TGRS2023	0.22	59.93	32.74	87.20	3.32
	DNA-Net	TIP2023	4.70	64.88	6.65	89.22	2.59
	ISTDU-Net	GRSL2022	2.75	65.71	26.58	90.57	1.37
2	LWNet	TGRS2023	-	67.55	161.00	90.23	3.6
2	RepISD	TGRS2023	-	66.38	58.17	88.55	1.49
	UIU-Net	TIP2023	50.54	65.69	22.49	91.24	1.34
	SpirDet-t	Ours	0.23	64.75	258.60	88.88	0.54
	SpirDet-s	Ours	0.28	67.46	208.96	88.55	1.21
	SpirDet-m	Ours	0.48	70.45	189.38	92.59	1.28

TABLE III: Our Model v.s. SOTAs: Comparison of Params(M), MIoU(%), FPS, $P_d(\%)$, and $F_a(\times 10^{-5})$ Values on the IRSTD-1K [31] Dataset. The best results are highlighted in bold, and the second are in underline. Methods classified under '1' are model-based, while those under '2' are data-driven.

B. Effectiveness of Our Approach

A comprehensive comparison was conducted between the proposed SpirDet and state-of-the-art methods, encompassing Top-Hat [16], Max-Median [17], RLCM [18], WSLCM [19], TLLCM [20], MSLCM [21], MSPCM [21], IPI [23], NRAM [24], RIPT [25], PSTNN [26], MSLSTIPT [27], ACM [29], ALCNet [30], ISNet [31], RDIAN [32], DNANet [33], IST-DUNet [34], LWNet [66], RepISD [67], UIUNet [35].

In Table III, various models were compared on the IRSTD-1K [31] dataset, characterized by the smallest target proportion and highest resolution. Notably, our SpirDet-m recorded a 70.45 MIoU, exceeding the previous best of 65.71 (ISTDU-Net) by approximately 4.74, with a 2-unit increase in P_a , a lower F_a , and an approximately sevenfold FPS advantage. And the model parameters were a mere 17% of ISTDU-Net.

Methods	Venue	Params		NUDT-S	IRST	
Methods	venue	Params	$MIoU \uparrow$	$FPS \uparrow$	$P_d \uparrow$	$F_a \downarrow$
Top-Hat	OE1996	-	20.72	-	78.40	16.67
Max-Median	SPIE1999	-	4.20	-	58.41	3.68
RLCM	GRSL2018	-	15.13	-	66.34	16.29
WSLCM	GRSL2021	-	0.84	-	74.57	5239.16
TLLCM	GRSL2019	-	7.05	-	62.01	4.61
MSLCM	IPT2018	-	6.64	-	56.82	2.56
MSPCM	IPT2018	-	5.85	-	55.86	11.59
IPI	TIP2013	-	17.75	-	74.48	4.12
NRAM	RS2018	-	6.93	-	56.40	1.92
RIPT	JSTARS2018	-	29.44	-	91.85	34.43
PSTNN	RS2019	-	14.84	-	66.13	4.41
MSLSTIPT	RS2023	-	8.34	-	47.39	8.81
ACM	WACV2021	0.40	64.85	330.64	96.72	2.85
ALCNet	TGRS2021	0.43	61.13	346.58	97.24	2.90
ISNet	CVPR2022	0.97	81.23	80.08	97.77	0.63
RDIAN	TGRS2023	0.22	82.41	121.89	98.83	1.36
DNA-Net	TIP2023	4.70	89.81	31.35	98.90	0.64
ISTDU-Net	GRSL2022	2.75	92.34	98.98	98.51	0.55
LWNet	TGRS2023	-	73.91	183.00	95.13	2.76
RepISD	TGRS2023	-	-	-	-	-
UIU-Net	TIP2023	50.54	90.51	54.17	98.83	0.83
SpirDet-lr	Ours	0.24	94.43	310.15	99.15	0.54

TABLE IV: Our Model v.s. SOTAs: Comparison of Params(M), MIoU(%), FPS, $P_d(\%)$, and $F_a(\times 10^{-5})$ Values on the NUDT-SIRST [33] Dataset.

The lighter SpirDet-t outperformed other lightweight networks in MIoU, reaching 258 FPS, with the lowest F_a among all models. In most indicators, our method emerged superior, boasting lower parameters and higher FPS. It verifies that our method's significant ability in high-resolution scenarios as shown in Fig.5.

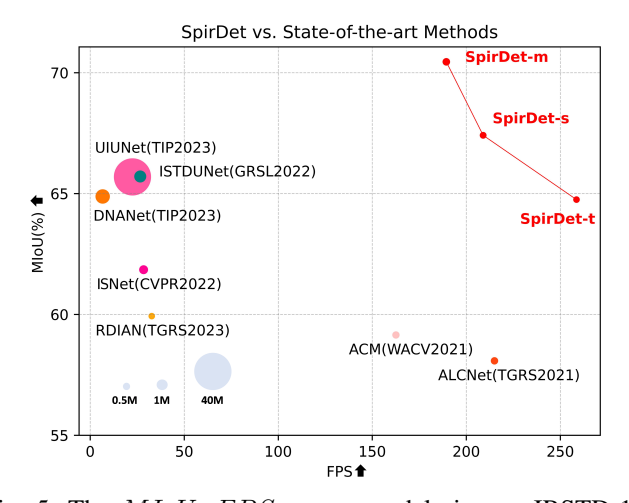


Fig. 5: The MIoU, FPS versus model size on IRSTD-1K [31] test set. Our SpirDet are marked as red point.

On the distinguishable NUDT-SIRST [33] dataset, as illustrated in Table IV, SpirDet was tested against the SOTA model. Our method yielded a 94.43 MIoU, 99.15 P_d , and 0.54 F_a , successively surpassing the previous best results by 2.09, 0.25, and 0.01, while maintaining an FPS nearly ten times higher than DNANet with the previous highest P_d .

In Table V, comparative experiments were performed between SpirDet and other deep learning-based networks on the SIRST3 and NUST [28] datasets. The trials demonstrated that our SpirDet nearly topped all performance indicators, all while maintaining excellent speed performance and minimal parameters.

The preceding results emphatically demonstrate SpirDet's superior model positioning ability $(P_d \text{ and } F_a)$ and detailed learning capacity (MIoU) in complex infrared scenes. Notably, even without resorting to additional acceleration techniques, our model's FPS can match or surpass prior lightweight networks. In addition, we also provide visual results on four datasets as shown in Fig.6, our proposed SpirDet not only avoids false detections, but also closely aligns the predicted small targets with the Ground Truth.

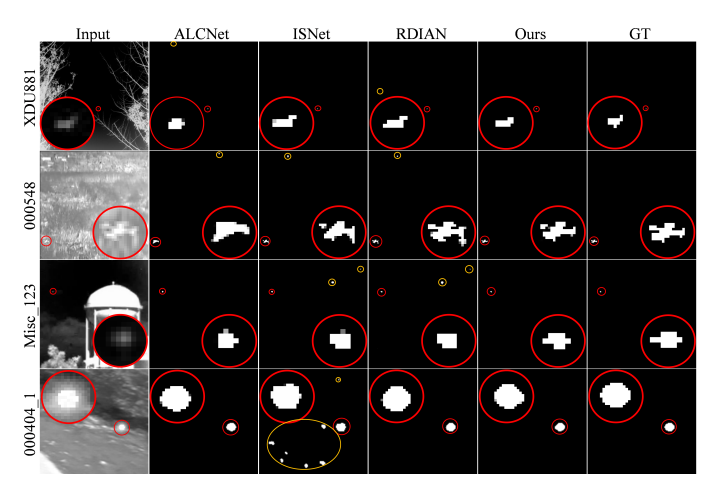


Fig. 6: Comparative Visualization of Various Networks on IRSTD-1K [31], NUDT-SIRST [33], NUAA-SIRST [29] and NUST [28] Datasets. The correct detected targets are highlighted in red and magnified, while misidentified targets are marked in yellow.

C. Ablation Studies

The impact of the sparsity ratio α in DBSD. Table VI demonstrates that α profoundly affects the outcomes, creating an almost monotonic variation in FPS, P_d , and F_a in response to changes in α . When α is reduced to 0.05%, it stringently confines the potential area of small targets. As expected, this results in a decrease in the false detection rate, F_a , of small targets, and an increase in FPS by curtailing the range the sparse head is required to caculate. Nevertheless, this leads to a decrease in the recall rate for small targets, causing MIoU and P_d to sharply decline to 38.63 and 75.42, respectively. On the contrary, an increase in α causes F_a to rise, but simultaneously leads to a swift decrease in the model's FPS, especially when DBSD is not employed, bringing FPS down to approximately 159. After α increases to 0.5%, MIoU and P_d reach a peak and then start to decline. This leads us to conjecture that α regulates the extent of contextual information for small targets, and an overexpansion of this extent may disrupt the model's learning of small target information. Additionally, we present the visualization results of the sparse graph to demonstrate the effectiveness of DBSD, as shown in Fig. 7.

The ablation studies of the DO-RepEncoder. In the Table VII, we evaluated the enhancements in GMACs and Params that reparameterization brings to SpirDet when applied via DO-RepEncoder. The empirical data indicates that reparameterization, on average, reduces the size of various models by

Methods	Venue	Params		SIRST	3			NUST	•			Averag	e	
Wiethous	venue	raianis	$MIoU \uparrow$	$FPS \uparrow$	$P_d \uparrow$	$F_a \downarrow$	$MIoU \uparrow$	$FPS \uparrow$	$P_d \uparrow$	$F_a \downarrow$	$MIoU \uparrow$	$FPS \uparrow$	$P_d \uparrow$	$F_a \downarrow$
ACM	WACV2021	0.40	57.98	272.15	86.67	1.29	79.95	294.67	91.22	0.63	68.97	283.41	88.95	0.96
ALCNet	TGRS2021	0.43	66.03	303.23	93.30	1.13	86.20	317.39	95.46	1.08	76.12	310.31	94.38	1.11
ISNet	CVPR2022	0.97	71.83	77.17	95.06	1.93	90.10	$\overline{114.24}$	96.27	0.22	80.97	95.71	95.67	1.08
RDIAN	TGRS2023	0.22	70.97	118.80	93.50	1.86	90.13	310.29	96.24	0.47	80.55	214.55	94.87	1.17
DNA-Net	TIP2023	4.70	75.67	30.57	96.14	1.27	88.79	71.22	96.68	0.73	82.23	50.90	96.41	1.00
ISTDU-Net	GRSL2022	2.75	79.18	98.76	96.07	0.70	91.05	112.29	97.41	0.39	85.12	105.53	96.74	0.55
LWNet	TGRS2023	-	67.39	-	92.95	5.56	86.07	-	94.73	3.03	76.73	-	93.84	4.30
RepISD	TGRS2023	-	-	-	-	-	92.47	-	97.56	0.28	-	-	-	-
UIÛ-Net	TIP2023	50.54	76.89	52.51	96.00	0.93	90.23	56.97	96.68	0.30	83.56	54.74	96.34	0.62
SpirDet-lr	Ours	0.28	82.45	250.42	96.54	0.78	<u>91.15</u>	369.05	<u>97.41</u>	0.32	86.80	<u>309.74</u>	96.98	0.55

TABLE V: Our Model v.s. SOTAs: Comparison of Params(M), MIoU(%), FPS, $P_d(\%)$, and $F_a(\times 10^{-5})$ Values on the SIRST3 and NUST [28] Datasets.

Metric		V	v/ DBSD			w/o DBSD
Wictife	α =0.05%	α =0.1%	α =0.5%	α =1%	α =5%	W/O DBSD
MIoU	38.63	49.56	70.45	69.39	68.64	67.17
FPS	204.29	191.30	189.38	178.76	173.79	159.64
P_d	75.42	80.80	92.59	91.24	89.22	89.56
F_a	0.34	1.218	1.28	2.226	3.28	3.16

TABLE VI: The influence of the hyperparameter α in DBSD on the experimental results over the IRSTD-1K [31] dataset.

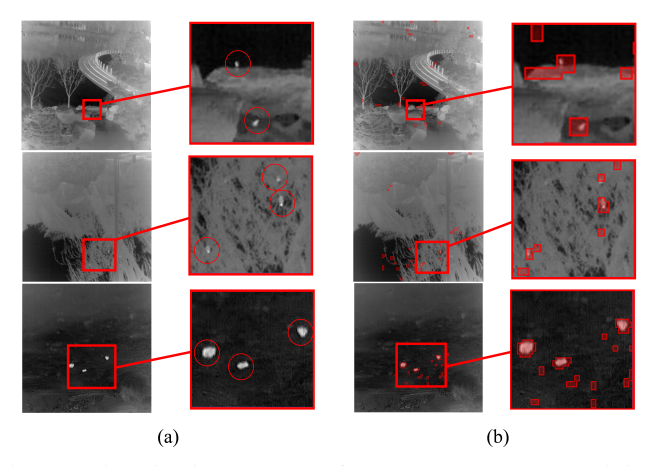


Fig. 7: Visualization results of the DBSD. (a)The original images with target locations denoted by red circles. (b)The DBSD's sparse graph, highlighting potential target locations with red zones.

a factor of 2.5. In terms of the GMACs metric the model demonstrates resource efficiency by saving more than twice the computational resources during the inference process. A separate ablation study on the downsampling orthogonality constraint within DO-RepEncoder is presented in Table VIII. The findings suggest that the downsampling orthogonality enhances MIoU by 0.5 and P_d by approximately 4. We typically configure DO-RepEncoder with a parallel convolution count, K, of 4, where the experiments confirm that optimal performance is attained when K is set to 4.

D. Discussions

Can the sparse operation replace the attention mechanism? The attention mechanism [3], [33] and sparse operations, commonly employed in infrared small target detection, possess both similarities and differences, as delineated in Table IX. As outlined in Sec. IV-C, the acquisition of excessive contextual

Methods	Params(M)			GMACs		
Michious	Before	After	Enhancement	Before	After	Enhancement
t	0.564	0.234	2.4×	1.862	0.617	3.0×
s	0.756	0.284	2.6×	2.310	0.807	2.9×
m	1.210	0.483	2.5 ×	2.688	1.210	2.2×

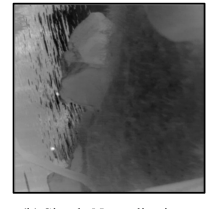
TABLE VII: Effects of Reparameterization on Params(M) and GMACs in RepirDet.

Methods	MIoU	P_d	F_a
RepEncoder w/ DO	70.4	92.6	1.3
RepEncoder w/o DO	69.9	88.8	1.2

TABLE VIII: The impact of Downsampling Orthogonality (DO) on the experimental results on the IRSTD-1K [31] dataset.

information may invite interference. Theoretically, sparse operations can facilitate learning of local contextual information related to the target, while focusing computations solely on potential target positions, thereby accelerating calculations. Thus, it may be a preferable alternative to the attention mechanism. To validate this, we substituted all the attention mechanisms in DNANet with sparse operations, and conducted experiments on the IRSTD-1K and SIRST-3 datasets as shown in Table X. The experimental outcomes reveal that the sparse version of DNANet either matches or surpasses the performance of the attention-based model, while notably enhancing inference speed.





(b) Simple Normalization

Fig. 8: Different normalization methods for input images.

Effects of different Normalizations. Typically, input images must be mapped to the range [0, 1]. Some infrared small target detectors independently computed the mean and variance of pixel values across different datasets as shown in Fig. 8(a), and normalized the input images using standardization. This strategy tends to homogenize the pixel value distributions across diverse images. However, standardization may result in diminished image hierarchy. Notably, when the small target

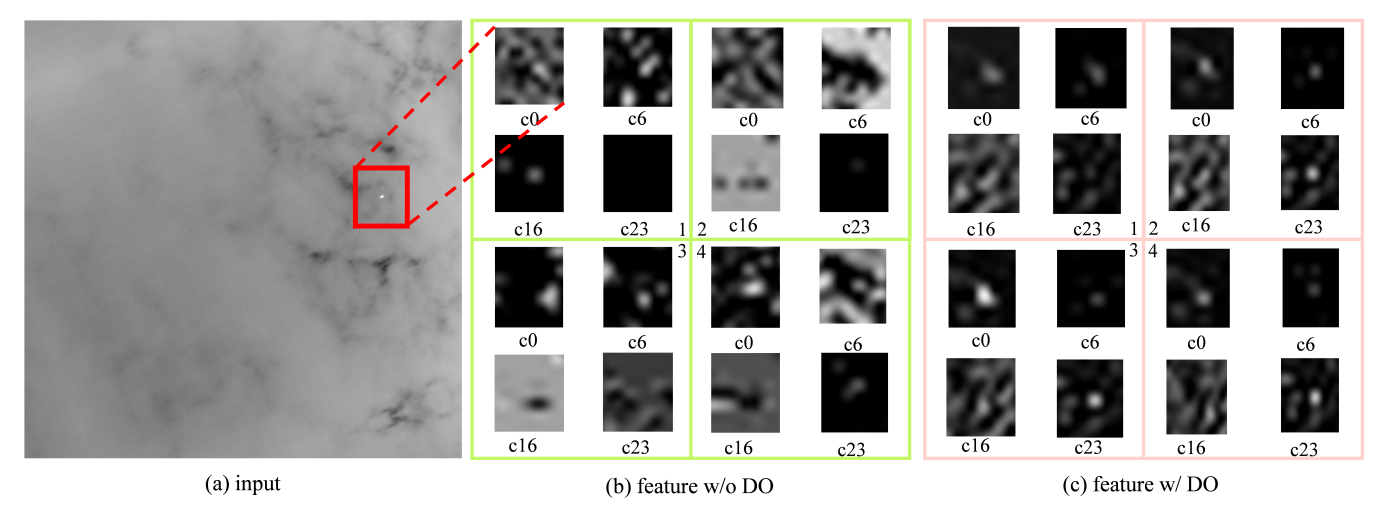


Fig. 9: Visualization of features around the target for K (K=4) parallel convolutions. (a) Target features when DO was not used. (b) Target features when using DO. '1', '2', '3', '4' represent different convolutions. 'c0' represents the 0_{th} channel.

Operator	Attention	Sparse
Context Learning	Self-adaption	Target-aware
Range	Global/Local	Local
Computation	Soft	Hard
Purpose	Relation Modeling	Target Kernel

TABLE IX: The similarities and differences of the attention mechanism and sparse operation in small target detection.

Dataset	Mechanism	MIoU	FPS	P_d	F_a
SIRST-3	Attention	74.5	30.0	95.9	1.4
31K31-3	Sparse	75.6	53.3	96.6	0.4
IRSTD-1K	Attention	64.8	6.6	89.2	2.6
IKS1D-1K	Sparse	64.1	18.3	89.2	1.3

TABLE X: The impact of the Attention mechanism and Sparse operation on DNA-Net on SIRST-3 and IRSTD-1K [31].

and the background exhibit minimal differences, the standardized small target risks being submerged in the background. Experimental results from Table XI indicate that a straightforward normalization approach, which divides the image by 255 easily as shown in Fig. 8(b), can more effectively maintain image hierarchy, thereby enhancing the distinguishability of small targets. Thus, we advocate for the use of simple normalization in replace of standardization to normalize input images.

	MIoU	P_d	F_a	
SpirDet-m	w/ Standardization	68.2	88.5	2.0
Spir Det-in	w/ SN	70.4	92.5	1.2

TABLE XI: The results of the two normalization methods on the IRSTD-1K [31] dataset. 'SN' denotes simple normalization.

Analysis of Downsampling Orthogonality. Fig. 9 visualizes the disparate features surrounding the target, extracted from the feature map X_2 after it has been processed by K (K=4) parallel downsampling convolutions. The visualization outcomes highlight two key observations. Firstly, the target features are notably distinct in the feature maps by the application of Downsampling Orthogonality (DO), whereas the feature maps

(without utilizing DO) contain a greater extent of background clutter. Secondly, in the features w/o DO, some channels exhibit a degradation of small target information to all-zero features, a situation not encountered when DO is implemented. In summary, the application of DO to K parallel downsampled convolutions not only effectively inhibits the disappearance of small-target features but also facilitates a more diverse encoding of these features. This enhances the model's capacity to learn features such as the shape of the small targets.

Feature		MIoU	P_d	F_a
	P5	68.1	87.5	0.9
SpirDet-m	P4	67.7	80.4	2.7
•	P3	70.4	92.6	1.3

TABLE XII: Comparison of MIoU(%), $P_d(\%)$, and $F_a(\times 10^{-5})$ with different layers serving as inputs to the fast branch.

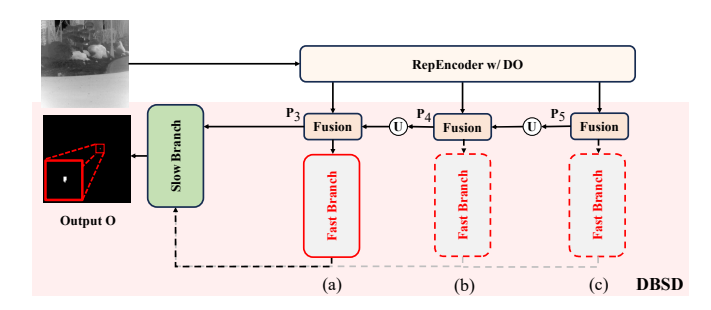


Fig. 10: Diagram of selecting different layers as input to the fast branch.

Which Layer is the Better Input of the Fast Branch? The role of the fast branch is to provide target potential locations for the refined refinement computation in the slow branch. Therefore, different scales of feature maps as inputs to the fast branch will result in different granularity of potential locations as shown in Fig. 10. In addition, Table XII illustrates the effect of using different resolution feature maps as input to

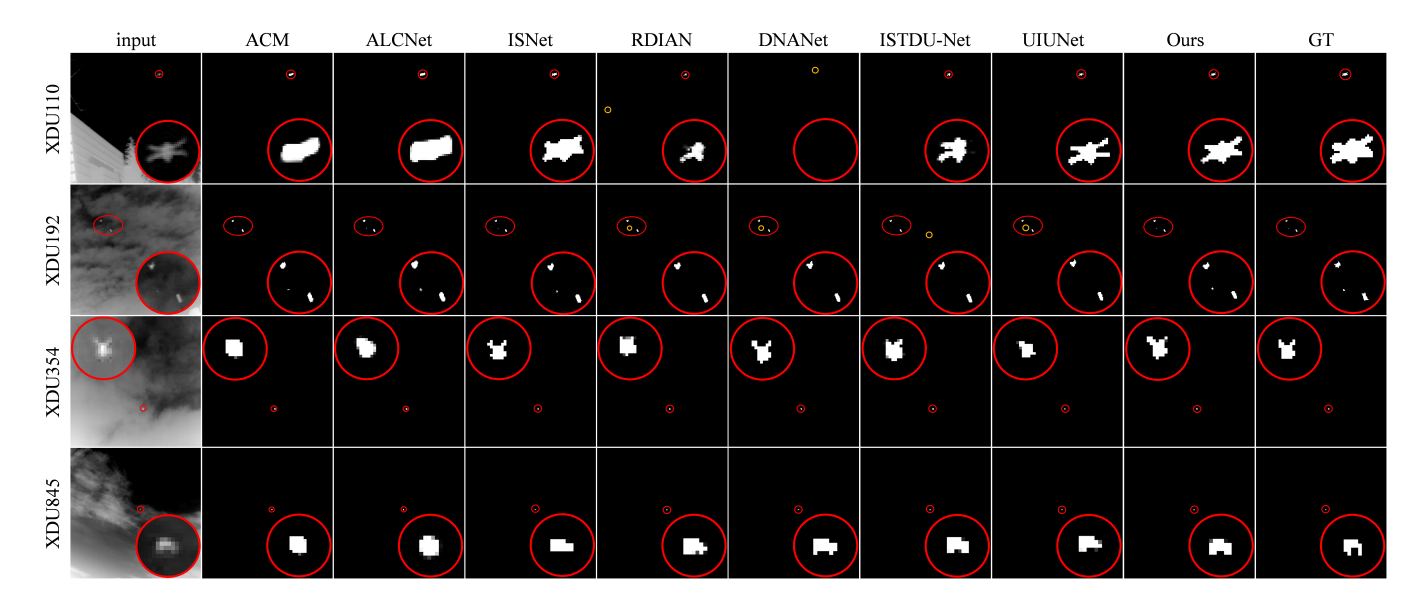


Fig. 11: Comparative visualization results covering ACM [29], ALCNet [30], ISNet [31], RDIAN [32], DNANet [33], ISTDU-Net [34], UIUNet [35] on IRSTD-1K [31] dataset. The correct detected targets are highlighted in red and magnified, while the misidentified targets are marked in yellow.

the fast branch. The granularity of potential locations varies with the resolution of the feature maps. Experimental results suggest that maximizing the resolution size of the fast branch, while maintaining a lower resolution, significantly improves outcomes.

More Visualization Results. Fig. 11 presents the visual results of the proposed method and the SOTA approaches on the IRSTD-1K [31] dataset. As illustrated, SpirDet has a much lower false detection rate, while learning a better shape of small targets. For instance, in XDU110, XDU354, and XDU845, although many networks are capable of recognizing the presence of small targets, our network exhibits a closer approximation to the Ground Truth (GT) in terms of shape fidelity. For example, the XDU192 image, our method can locate all the small targets whileas the compared methods exhibit omissions. The sparse potential target location regions obtained by DBSD are shown in Fig. 12. All the targets are truly identified by DBSD. Meanwhile, many possible target location regions are likewise used as candidate regions, which guarantees the recall rate of SpirDet.

V. CONCLUSION

In this paper, we introduce SpirDet, a novel approach tailored for infrared small target detection. Leveraging sparsity and a reparameterization mechanism, SpirDet efficiently detect small targets on high-resolution feature maps at a lower computational cost. Experimental results on multiple public datasets show that the SpirDet significantly enhancing inference speed while maintaining performance on the four public datasets . In the future, the sparsity and reparameterization mechanisms are expected to be applied in video sequences for detecting infrared small targets.

REFERENCES

- [1] K. Zhang, S. Ni, D. Yan, and A. Zhang, "Review of dim small target detection algorithms in single-frame infrared images," in In IEEE Advanced Information Management, Communicates, Electronic and Automation Control Conference (IMCEC), vol. 4, 2021, pp. 2115– 2120.
- [2] M. Zhao, W. Li, L. Li, J. Hu, P. Ma, and R. Tao, "Single-frame infrared small-target detection: A survey," *IEEE Geoscience and Remote Sensing Magazine*, vol. 10, no. 2, pp. 87–119, 2022.
- [3] A. Vaswani, N. Shazeer, N. Parmar, J. Uszkoreit, L. Jones, A. N. Gomez, and e. a. Kaiser, Łukasz, "Attention is all you need," *Advances in Neural Information Processing Systems*, vol. 30, 2017.
- [4] S. S. Rawat, S. K. Verma, and Y. Kumar, "Review on recent development in infrared small target detection algorithms," *Procedia Computer Science*, vol. 167, pp. 2496–2505, 2020.
- [5] R. Kou, C. Wang, Z. Peng, Z. Zhao, Y. Chen, J. Han, F. Huang, Y. Yu, and Q. Fu, "Infrared small target segmentation networks: A survey," *Pattern Recognition*, vol. 143, p. 109788, 2023. [Online]. Available: https://www.sciencedirect.com/science/article/pii/S0031320323004867
- [6] M. Zhang, H. Bai, J. Zhang, R. Zhang, C. Wang, J. Guo, and X. Gao, "Rkformer: Runge-kutta transformer with random-connection attention for infrared small target detection," in *Proceedings of the 30th ACM International Conference on Multimedia*(ACM MM), 2022, pp. 1730–1738
- [7] M. Zhang, K. Yue, J. Zhang, Y. Li, and X. Gao, "Exploring feature compensation and cross-level correlation for infrared small target detection," in *Proceedings of the 30th ACM International Conference on Multimedia*, 2022, pp. 1857–1865.
- [8] D. Pang, P. Ma, Y. Feng, T. Shan, R. Tao, and Q. Jin, "Tensor spectral k-support norm minimization for detecting infrared dim and small target against urban backgrounds," *IEEE Transactions on Geoscience and Remote Sensing*, vol. 61, pp. 1–13, 2023.
- [9] H. Wang, C. Liu, C. Ma, and S. Ma, "A novel and high-speed local contrast method for infrared small-target detection," *IEEE Geoscience* and Remote Sensing Letters, vol. 17, no. 10, pp. 1812–1816, 2019.
- [10] C. Yu, Y. Liu, S. Wu, Z. Hu, X. Xia, D. Lan, and X. Liu, "Infrared small target detection based on multiscale local contrast learning networks," *Infrared Physics & Technology*, vol. 123, p. 104107, 2022.
- [11] Z. Zuo, X. Tong, J. Wei, S. Su, P. Wu, R. Guo, and B. Sun, "Affpn: attention fusion feature pyramid network for small infrared target detection," *Remote Sensing*, vol. 14, no. 14, p. 3412, 2022.
- [12] T. Ma, Z. Yang, J. Wang, S. Sun, X. Ren, and U. Ahmad, "Infrared small target detection network with generate label and feature mapping," *IEEE Geoscience and Remote Sensing Letters*, vol. 19, pp. 1–5, 2022.

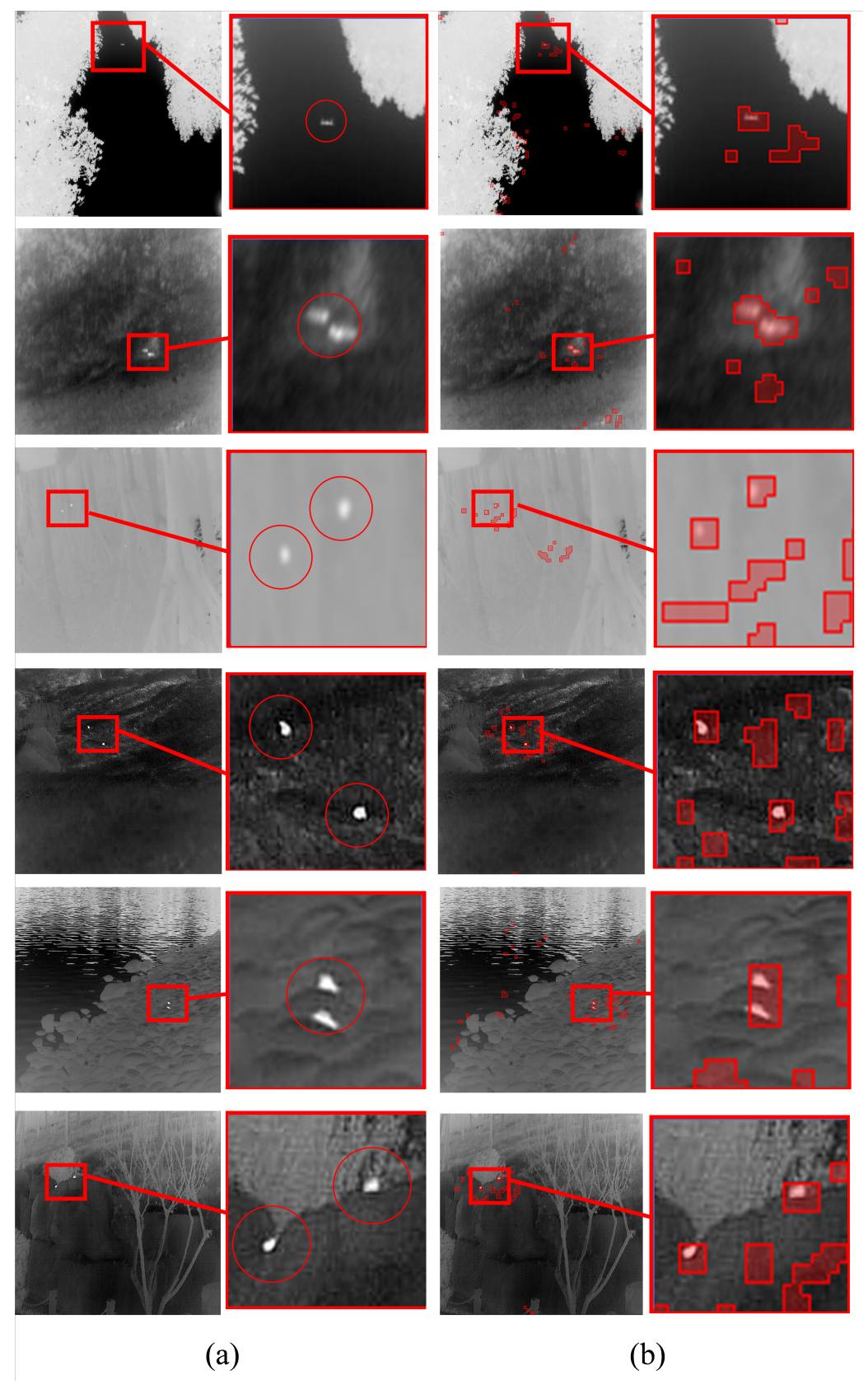


Fig. 12: More visualization results of the proposed DBSD. (a)The original images with target locations denoted by red circles. (b)The DBSD's sparse graph, highlighting potential target locations with red zones.

- [13] L. Zhang, H. Miao, J. Chen, W. Lin, R. Xu, and D. Zhang, "Research on infrared dim and small target detection algorithm based on frequency domain difference," *International Journal of Remote Sensing*, vol. 43, no. 8, pp. 2942–2964, 2022.
- [14] D. Yang, Z. Bai, and J. Zhang, "Infrared weak and small target detection based on top-hat filtering and multi-feature fuzzy decision-making," *Electronics*, vol. 11, no. 21, p. 3549, 2022.
- [15] O. Ronneberger, P. Fischer, and T. Brox, "U-net: Convolutional networks for biomedical image segmentation," in *Medical Image Computing* and Computer-Assisted Intervention—MICCAI 2015: 18th International Conference, Munich, Germany, October 5-9, 2015, Proceedings, Part III 18. Springer, 2015, pp. 234–241.
- [16] V. T. Tom, T. Peli, M. Leung, and J. E. Bondaryk, "Morphology-based algorithm for point target detection in infrared backgrounds," in *Signal and Data Processing of Small Targets 1993*, O. E. Drummond, Ed., vol. 1954, International Society for Optics and Photonics. SPIE, 1993, pp. 2 11. [Online]. Available: https://doi.org/10.1117/12.157758
- [17] S. D. Deshpande, M. H. Er, R. Venkateswarlu, and P. Chan, "Max-mean and max-median filters for detection of small targets," in *Signal and Data Processing of Small Targets 1999*, O. E. Drummond, Ed., vol. 3809, International Society for Optics and Photonics. SPIE, 1999, pp. 74 83. [Online]. Available: https://doi.org/10.1117/12.364049
- [18] J. Han, K. Liang, B. Zhou, X. Zhu, J. Zhao, and L. Zhao, "Infrared small target detection utilizing the multiscale relative local contrast measure," *IEEE Geoscience and Remote Sensing Letters*, vol. 15, no. 4, pp. 612– 616, 2018.
- [19] J. Han, S. Moradi, I. Faramarzi, H. Zhang, Q. Zhao, X. Zhang, and N. Li, "Infrared small target detection based on the weighted strengthened local contrast measure," *IEEE Geoscience and Remote Sensing Letters*, vol. 18, no. 9, pp. 1670–1674, 2021.
- [20] J. Han, S. Moradi, I. Faramarzi, C. Liu, H. Zhang, and Q. Zhao, "A local contrast method for infrared small-target detection utilizing a tri-layer window," *IEEE Geoscience and Remote Sensing Letters*, vol. 17, no. 10, pp. 1822–1826, 2020.
- [21] S. Moradi, P. Moallem, and M. F. Sabahi, "A false-alarm aware methodology to develop robust and efficient multi-scale infrared small target detection algorithm," *Infrared Physics & Technology*, vol. 89, pp. 387–397, 2018. [Online]. Available: https://www.sciencedirect.com/ science/article/pii/S1350449517302013
- [22] —, "A false-alarm aware methodology to develop robust and efficient multi-scale infrared small target detection algorithm," *Infrared Physics & Technology*, vol. 89, pp. 387–397, 2018. [Online]. Available: https://www.sciencedirect.com/science/article/pii/S1350449517302013
- [23] C. Gao, D. Meng, Y. Yang, Y. Wang, X. Zhou, and A. G. Hauptmann, "Infrared patch-image model for small target detection in a single image," *IEEE Transactions on Image Processing*, vol. 22, no. 12, pp. 4996–5009, 2013.
- [24] L. Zhang, L. Peng, T. Zhang, S. Cao, and Z. Peng, "Infrared small target detection via non-convex rank approximation minimization joint 12,1 norm," *Remote Sensing*, vol. 10, no. 11, 2018. [Online]. Available: https://www.mdpi.com/2072-4292/10/11/1821
- [25] Y. Dai and Y. Wu, "Reweighted infrared patch-tensor model with both nonlocal and local priors for single-frame small target detection," *IEEE Journal of Selected Topics in Applied Earth Observations and Remote Sensing*, vol. 10, no. 8, pp. 3752–3767, 2017.
- [26] L. Zhang and Z. Peng, "Infrared small target detection based on partial sum of the tensor nuclear norm," *Remote Sensing*, vol. 11, no. 4, 2019. [Online]. Available: https://www.mdpi.com/2072-4292/11/4/382
- [27] J. Han, S. Moradi, I. Faramarzi, H. Zhang, Q. Zhao, X. Zhang, and N. Li, "Infrared small target detection based on the weighted strengthened local contrast measure," *IEEE Geoscience and Remote Sensing Letters*, vol. 18, no. 9, pp. 1670–1674, 2020.
- [28] H. Wang, L. Zhou, and L. Wang, "Miss detection vs. false alarm: Adversarial learning for small object segmentation in infrared images," in *Proceedings of the IEEE/CVF International Conference on Computer Vision*, 2019, pp. 8509–8518.
- [29] Y. Dai, Y. Wu, F. Zhou, and K. Barnard, "Asymmetric contextual modulation for infrared small target detection," in *IEEE Winter Conference* on Applications of Computer Vision, WACV 2021, 2021.
- [30] Y. Dai, Y. Wu, F. Zhou, and K. Barnard, "Attentional Local Contrast Networks for Infrared Small Target Detection," *IEEE Transactions on Geoscience and Remote Sensing*, pp. 1–12, 2021.
- [31] M. Zhang, R. Zhang, Y. Yang, H. Bai, J. Zhang, and J. Guo, "Isnet: Shape matters for infrared small target detection," in *Proceedings of the IEEE/CVF Conference on Computer Vision and Pattern Recognition*, 2022, pp. 877–886.

- [32] H. Sun, J. Bai, F. Yang, and X. Bai, "Receptive-field and direction induced attention network for infrared dim small target detection with a large-scale dataset irdst," *IEEE Transactions on Geoscience and Remote* Sensing, vol. 61, pp. 1–13, 2023.
- [33] B. Li, C. Xiao, L. Wang, Y. Wang, Z. Lin, M. Li, W. An, and Y. Guo, "Dense nested attention network for infrared small target detection," *IEEE Transactions on Image Processing*, vol. 32, pp. 1745–1758, 2022.
- [34] Q. Hou, L. Zhang, F. Tan, Y. Xi, H. Zheng, and N. Li, "Istdu-net: Infrared small-target detection u-net," *IEEE Geoscience and Remote Sensing Letters*, vol. 19, pp. 1–5, 2022.
- [35] X. Wu, D. Hong, and J. Chanussot, "Uiu-net: U-net in u-net for infrared small object detection," *IEEE Trans. Image. Process.*, vol. 32, pp. 364– 376, 2023.
- [36] C. L. P. Chen, H. Li, Y. Wei, T. Xia, and Y. Y. Tang, "A local contrast method for small infrared target detection," *IEEE Transactions* on Geoscience and Remote Sensing, vol. 52, no. 1, pp. 574–581, 2014.
- [37] C. Guo, Q. Ma, and L. Zhang, "Spatio-temporal saliency detection using phase spectrum of quaternion fourier transform," in 2008 IEEE Conference on Computer Vision and Pattern Recognition, 2008, pp. 1–8.
- [38] Y. He, M. Li, J. Zhang, and Q. An, "Small infrared target detection based on low-rank and sparse representation," *Infrared Physics & Technology*, vol. 68, pp. 98–109, 2015. [Online]. Available: https://www.sciencedirect.com/science/article/pii/S1350449514002576
- [39] K. Wang, S. Du, C. Liu, and Z. Cao, "Interior attention-aware network for infrared small target detection," *IEEE Transactions on Geoscience* and Remote Sensing, vol. 60, pp. 1–13, 2022.
- [40] X. Tong, B. Sun, J. Wei, Z. Zuo, and S. Su, "Eaau-net: Enhanced asymmetric attention u-net for infrared small target detection," *Remote Sensing*, vol. 13, no. 16, p. 3200, 2021.
- [41] T. Ma, Z. Yang, B. Liu, and S. Sun, "A lightweight infrared small target detection network based on target multiscale context," *IEEE Geoscience* and Remote Sensing Letters, vol. 20, pp. 1–5, 2023.
- [42] M. Zhang, R. Zhang, J. Zhang, J. Guo, Y. Li, and X. Gao, "Dim2clear network for infrared small target detection," *IEEE Transactions on Geoscience and Remote Sensing*, vol. 61, pp. 1–14, 2023.
- [43] M. Long, S. Cong, H. Shanshan, W. Zoujian, W. Xuhao, and W. Yanxi, "Sddnet: Infrared small and dim target detection network," CAAI Transactions on Intelligence Technology, vol. n/a, no. n/a. [Online]. Available: https://ietresearch.onlinelibrary.wiley.com/doi/abs/ 10.1049/cit2.12165
- [44] J. Moran and H. Qing, "Brain-inspired filtering network for small infrared target detection," *Multimedia Tools Appl.*, vol. 82, no. 18, p. 28405–28426, mar 2023. [Online]. Available: https://doi.org/10.1007/s11042-023-14762-x
- [45] T. Zhao, J. Cao, Q. Hao, C. Bao, and M. Shi, "Res-swintransformer with local contrast attention for infrared small target detection," *Remote Sensing*, vol. 15, no. 18, 2023. [Online]. Available: https://www.mdpi.com/2072-4292/15/18/4387
- [46] Y. Dai, X. Li, F. Zhou, Y. Qian, Y. Chen, and J. Yang, "One-stage cascade refinement networks for infrared small target detection," *IEEE Transactions on Geoscience and Remote Sensing*, vol. 61, pp. 1–17, 2023.
- [47] Q. Shi, C. Zhang, Z. Chen, F. Lu, L. Ge, and S. Wei, "An infrared small target detection method using coordinate attention and feature fusion," *Infrared Physics & Technology*, vol. 131, p. 104614, 2023. [Online]. Available: https://www.sciencedirect.com/science/article/pii/ S1350449523000725
- [48] C. Dang, Z. Li, C. Hao, and Q. Xiao, "Infrared small marine target detection based on spatiotemporal dynamics analysis," *Remote Sensing*, vol. 15, no. 5, 2023. [Online]. Available: https://www.mdpi. com/2072-4292/15/5/1258
- [49] C. Li, Z. Huang, X. Xie, and W. Li, "Ist-transnet: Infrared small target detection based on transformer network," *Infrared Physics & Technology*, vol. 132, p. 104723, 2023.
- [50] Z. Lu, Z. Huang, Q. Song, H. Ni, and K. Bai, "Infrared small target detection based on joint local contrast measures," *Optik*, vol. 273, p. 170437, 2023. [Online]. Available: https: //www.sciencedirect.com/science/article/pii/S0030402622016953
- [51] X. Zhang, Z. Yang, F. Shi, Y. Yang, and M. Zhao, "Infrared small target detection based on singularity analysis and constrained random walker," *IEEE Journal of Selected Topics in Applied Earth Observations and Remote Sensing*, vol. 16, pp. 2050–2064, 2023.
- [52] G. Zhang, A. Hamdulla, and H. Ma, "Infrared small target detection based on multidirectional cumulative measure," *IEEE Geoscience and Remote Sensing Letters*, vol. 20, pp. 1–5, 2023.

- [53] J. Liu, J. Zhang, Y. Wei, and L. Zhang, "Infrared small target detection based on multidirectional gradient," *IEEE Geoscience and Remote Sensing Letters*, vol. 20, pp. 1–5, 2023.
- [54] S. Du, K. Wang, and Z. Cao, "Bpr-net: Balancing precision and recall for infrared small target detection," *IEEE Transactions on Geoscience* and Remote Sensing, vol. 61, pp. 1–15, 2023.
- [55] J. Peng, H. Zhao, K. Zhao, Z. Wang, and L. Yao, "Courtnet: Dynamically balance the precision and recall rates in infrared small target detection," *Expert Systems with Applications*, vol. 233, p. 120996, 2023. [Online]. Available: https://www.sciencedirect.com/ science/article/pii/S0957417423014987
- [56] J. Peng, H. Zhao, Z. Hu, K. Zhao, and Z. Wang, "Dynamic background reconstruction via transformer for infrared small target detection," *ArXiv* Preprint arXiv:2301.04497, 2023.
- [57] C. Yang, Z. Huang, and N. Wang, "Querydet: Cascaded sparse query for accelerating high-resolution small object detection," in *Proceedings of* the IEEE/CVF Conference on Computer Vision and Pattern Recognition, 2022, pp. 13668–13677.
- [58] Y. Yan, Y. Mao, and B. Li, "Second: Sparsely embedded convolutional detection," *Sensors*, vol. 18, no. 10, 2018. [Online]. Available: https://www.mdpi.com/1424-8220/18/10/3337
- [59] B. Du, Y. Huang, J. Chen, and D. Huang, "Adaptive sparse convolutional networks with global context enhancement for faster object detection on drone images," in *Proceedings of the IEEE/CVF Conference on Computer Vision and Pattern Recognition*, 2023, pp. 13435–13444.
- [60] T. Verelst and T. Tuytelaars, "Dynamic convolutions: Exploiting spatial sparsity for faster inference," in *Proceedings of the IEEE/CVF Confer*ence on Computer Vision and Pattern Recognition, 2020, pp. 2320–2329.
- [61] T.-Y. Lin, P. Dollár, R. Girshick, K. He, B. Hariharan, and S. Belongie, "Feature pyramid networks for object detection," in *Proceedings of the IEEE Conference on Computer Vision and Pattern Recognition*, 2017, pp. 2117–2125.
- [62] X. Ding, X. Zhang, N. Ma, J. Han, G. Ding, and J. Sun, "Repvgg: Making vgg-style convnets great again," in *Proceedings of the IEEE/CVF Conference on Computer Vision and Pattern Recognition*, 2021, pp. 13733–13742.
- [63] P. K. A. Vasu, J. Gabriel, J. Zhu, O. Tuzel, and A. Ranjan, "Mobileone: An improved one millisecond mobile backbone," in *Proceedings of the IEEE/CVF Conference on Computer Vision and Pattern Recognition*, 2023, pp. 7907–7917.
- [64] A. Brock, J. Donahue, and K. Simonyan, "Large scale gan training for high fidelity natural image synthesis," ArXiv Preprint arXiv:1809.11096, 2018.
- [65] A. Brock, T. Lim, J. M. Ritchie, and N. Weston, "Neural photo editing with introspective adversarial networks," ArXiv Preprint arXiv:1609.07093, 2016.
- [66] R. Kou, C. Wang, Y. Yu, Z. Peng, M. Yang, F. Huang, and Q. Fu, "Lw-irstnet: Lightweight infrared small target segmentation network and application deployment," *IEEE Transactions on Geoscience and Remote Sensing*, 2023.
- [67] S. Wu, C. Xiao, L. Wang, Y. Wang, J. Yang, and W. An, "Repisd-net: Learning efficient infrared small-target detection network via structural re-parameterization," *IEEE Transactions on Geoscience and Remote Sensing*, 2023.